Crystallization Behavior of Polyamide-6 Microcellular Nanocomposites*

MINGJUN YUAN, LIH-SHENG TURNG,† SHAOQIN GONG AND ANDREAS WINARDI
Polymer Engineering Center
Department of Mechanical Engineering
University of Wisconsin-Madison
Madison, WI 53706, USA

DANIEL CAULFIELD
USDA Forest Products Laboratory
Madison, WI 53726, USA

ABSTRACT: The crystallization behaviors of polyamide-6 (PA-6) and its nanocomposites undergoing the microcellular injection molding process are studied using Transmission Electron Microscopy (TEM), X-ray Diffractometer (XRD), Polarized Optical Microscopy (POM), and Differential Scanning Calorimetry (DSC). The relationships among the morphology, the mechanical property of the molded parts, and the crystallization behavior are investigated. With the addition of nanoclays in microcellular injection molded parts, the growth of the α-form crystal is suppressed and the formation of γ-form crystals is promoted. Both nanoclay and dissolved gas have a big influence on PA-6 crystalline structures. The existence of nanoclay increases the initial crystallization rate. But with extra addition of nanoclays in the polymer matrix, the increase of crystallization rate is reduced. Microcellular injection molded nanocomposites with proper amount of nanoclays possess the maximum crystallization activation energy and produce a finer and denser microcell structure which leads to better mechanical properties.

KEY WORDS: microcellular injection molding, polyamide-6, nanocomposite, crystallization, montmorillonite (MMT).

---

*This paper was presented at ANTEC 2004, Chicago, Illinois, May 16-20, and the copyright is held by the Society of Plastic Engineers.
†Author to whom correspondence should be addressed.

0021-955X/04/05 0397-13 $10.00/0 DOI: 0.1177/0021955X04047220

INTRODUCTION

Introducing layered organosilicate platelets into a polymer matrix produces unique composite materials, which offer improved stiffness, heat resistance, barrier and flame retardation, and improved dimensional stability with a small clay load (<10%). By injecting 'supercritical' N_2 or CO_2 into the machine barrel to create a single-phased polymer-gas solution, a microcellular structure (microcells of 1–100μm) can be made by using lower injection pressure, shorter cycle time, and less material. It eliminates the need for packing pressure, and improves the dimensional stability of the molded parts. Microcells also greatly enhance the part toughness of many brittle polymeric materials by acting as crack arrestors. Much interest has been generated to study the synergistic benefits of integrating both types of technologies in a single molding process and the relationships among molding parameters, morphology, and property of the molded parts.

As PA-6, nanoclay, and dissolved N_2 or CO_2 all have large impacts on the molding condition and final property of the molded part, the relationships between the molding parameters, morphology, and property of the molded parts are especially complicated. As PA-6–nanoclay and PA-6 present different crystalline structures, the differences in the mechanical behavior of these two materials could be related to the reinforcing nanofiller and/or the difference in the crystalline structure. The relative importance of these two contributions is still unknown. Bureau et al. studied the role of crystallinity and reinforcement in the mechanical behavior of PA-6 nanocomposite and pointed out that it is the reinforcing nanofillers and not the modification of the crystallinity that is responsible for the improved mechanical performance [1]. In spite of this and the report which showed that the crystallization rate of certain polymers was slowed by the presence of CO_2 [2], PA-6 and PA-6 nanocomposite crystallization behavior in the microcellular injection molding process is still not known. The objective of this work is to try to understand the crystallization behavior that eventually determines the structure and property of the molded part.

EXPERIMENTAL

PA-6–clay nanocomposites with two different loading levels of montmorillonite (MMT) organoclays, 5.0wt% and 7.5wt%, (designated as NC2 and NC3, respectively) and their corresponding base PA-6 resin (symbolized as BR2) were supplied by the RTP Company (USA). These materials were dried for 4 h at 100°C under vacuum to remove moisture

before use. The materials were injection molded using a 150-ton injection-molding machine equipped with microcellular injection molding capability. The experiments were based on the L9 orthogonal array design. The L9 experiments contain four different operational variables at three different levels, that is, in the order of melt temperature (232, 243, and 254°C), supercritical fluid content (0.2, 0.4, and 0.6wt%), shot size (16.5, 18.4, and 20.5 mm), and injection speed (20, 40, and 60%).

Transmission Electron Microscope (JOEL JEM100CX TEM and LEO 912 EFTEM), Customized Leitz Orthotlan-POL Polarized Optical Microscopy (Ernst Leitz Wetzlar GMBH), X-ray Diffraction (XRD, STOE high resolution X-ray diffractometer with Cu Kα radiation at 40 kV and 25 mA), Differential Scanning Calorimeters (DSC, Perkin Elmer DSC-7, and Netzsch DSC 200 PC) were used to analyze the specimens from microcellular injection molding and/or compression molded Specimens and the as-received raw materials.

Transmission electron microscope scanning of the specimens from as-received materials were performed on JOEL JEM100CX TEM. TEM tests of the specimens from cross-sectioning the block of injection molded samples with an ultratome were performed on LEO 912 EFTEM with the use of the objective aperture and the energy filter.

The POM specimens were made by compression molding the molten raw materials and cooling them into solid films of 10 μm thickness on a hot stage. The compression molded specimens involved both slow and fast cooling rates, which were made by cooling the sample from 255°C to room temperature on the hot stage and by cooling the samples in air, respectively. The injection molded specimens were microtomed to make the POM film specimens of 10 μm thickness.

The XRD specimens were prepared in two different ways: by compression molding the raw materials at different cooling rates and by cutting and fine-polishing the injection molded samples. During the compression molding, each material was held at 255°C for 6 min. The fast, intermediate, and slow cooling rates were controlled by cooling the molds from 255 to 150°C for 6-8, 20, and 60 min, respectively.

All the DSC thermal analysis experiments were carried out under a nitrogen atmosphere. The specimens from as-received materials underwent the nonisothermal and isothermal cooling DSC testing, respectively. To eliminate the thermal and stress histories of these specimens, each specimen was heated to 255°C at 10°C/min and stabilized for 6 min before conducting the tests. For cubic specimens cut from the skin and the core of the injection molded samples, only heating was executed. The weights of the samples are between 10 and 11 mg.

RESULTS AND DISCUSSION

PA-6 microcellular nanocomposite exhibits a great difference in mechanical properties from its PA-6 microcellular counterpart under the same injection molding condition. From Figure 1, it can be seen that even with the same material, different microcellular molding condition produces a big difference in mechanical properties, as reported earlier [3]. The property difference relates to the morphologies, the contents of nanoclays and dissolved N_2 in PA-6 matrix, and the molding conditions of the parts. Typical cell density of PA-6 microcellular nanocomposite could be 100 times higher than that of its PA-6 microcellular counterpart, with cell size fivefold smaller. Furthermore, the microcells in PA-6 microcellular nanocomposite have a smooth cell wall surface whereas that of PA-6 microcellular part is usually much rougher, as shown in Figures 2 and 3 [3].

The TEM images from JOEL JEM100CX TEM show that the nanoclays in NC2 and NC3 nanocomposites were relatively well-dispersed in polymer matrices, even though some small clay decks still existed.

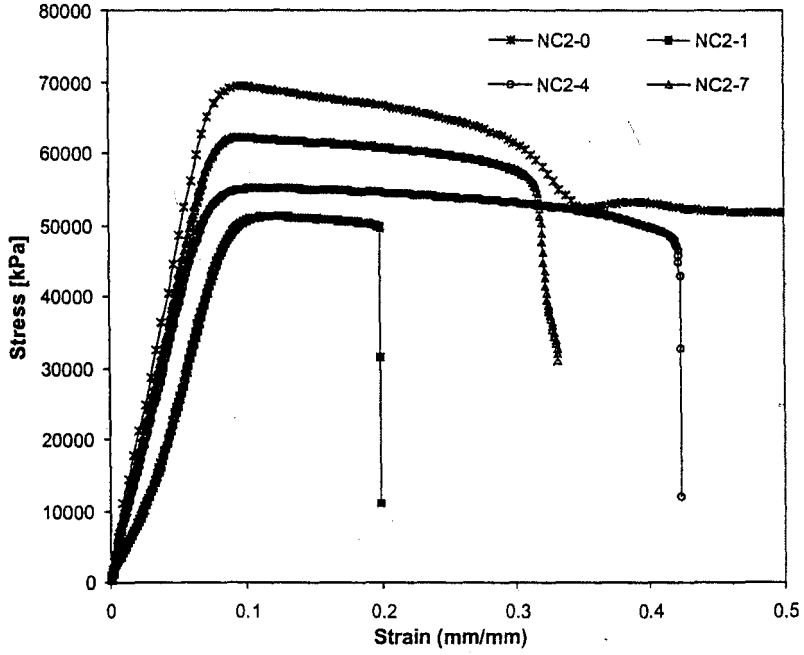

Figure 1. The mechanical properties of microcellular nanocomposites molded under different conditions in comparison with solid injection molded nanocomposite specimen (NC2-0).

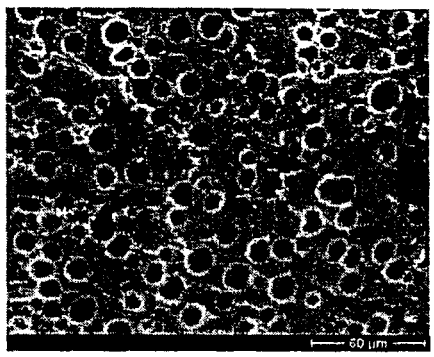

Figure 2. The scanning electron micrograph of microcells in PA-6 microcellular nanocomposite part.

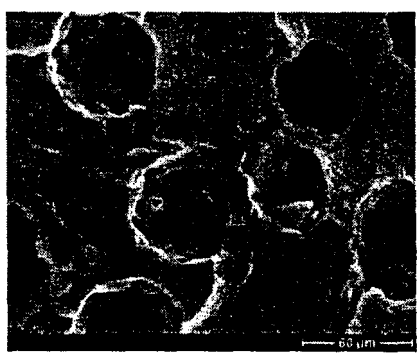

Figure 3. The scanning electron micrograph of microcells in PA-6 microcellular part.

As expected, more clay platelets can be seen in the specimen of NC3 than in the specimen of NC2 (Figures 4 and 5).

Differential scanning calorimetry results for the BR2 microcellular injection molded specimens indicate that both the skin and the core regions have the strong melting endothermic peak around 222.4°C, which corresponds to the a-form of crystals. The areas under the peak curves show that the core region which experienced the slower cooling rate had the higher crystallinity (Figure 6). On the other hand, the core and the skin regions of NC2 microcellular specimens show a relatively weaker a-form crystal formation. An endothermic peak or a small endothermic shoulder appeared around 212.4°C, which is associated with the crystalline γ-form. Note that the melting peak is broadened at the skin region. This reflects the changes in crystallite thickness and its distribution. Despite the faster initial crystallization rate, which will be

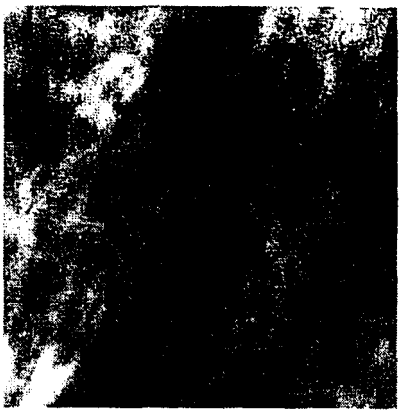

Figure 4. The transmission electron micrograph of the nanocomposite with 5% MMT.

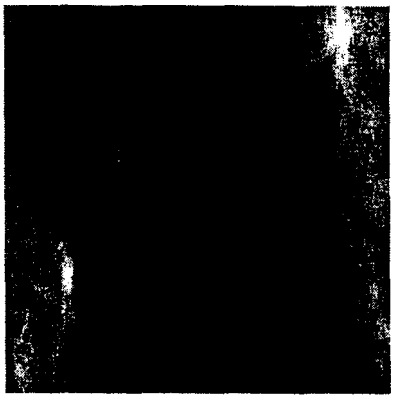

Figure 6. The transmission electron micrograph of the nanocomposite with 7.5% MMT.

discussed later, a lower level of crystallinity is seen in these microcellular nanocomposite specimens.

Polarized optical microscopy results show that under the fast cooling condition, the structure of PA-6 is more likely to be spherulitic but that of PA-6 nanocomposite is hard to see. With slow cooling rate, the spherulite of PA-6 usually impinges with its neighboring ones, and the structure of PA-6 nanocomposite is likely to be irregular, as shown in Figure 7. The sizes of the spherulitic structures in microcellular specimens are obviously smaller than those in solid specimens, but they are all much smaller than those in hot-stage specimens. Meanwhile, the much smaller and denser crystalline structures are present in NC2 molded specimens. POM results also verified that the crystalline

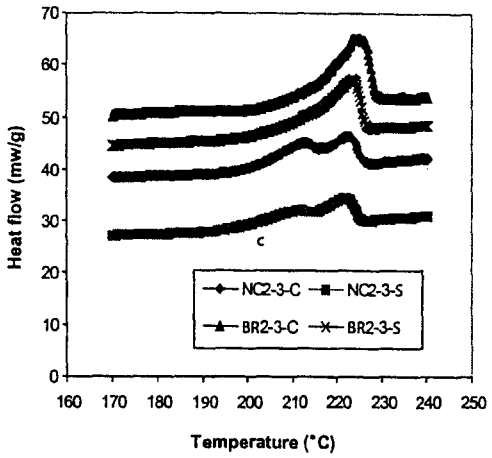

Figure 6. DSC thermal graphs of the injection molded skin (S) and core (C) specimens from Molding Trial No. 3.

structures on the microcell wall surface are the same as those of the microcell surrounding solid material. This implies that the crystallization behavior of PA-6 and PA-6 nanocomposite strongly affect the smoothness and morphology of the microcells. Interestingly, at the skin region or at the corner of the two skin regions of BR2 microcellular injection molded sample, single spherulites can be clearly seen. Towards the center of the specimen, each spherulite becomes bigger and may impinge with, others. This demonstrates a large difference in the thermal histories between the boundary layer and the central part of the specimen. The molding condition for these kinds of samples is at the intermediate level (Level 2) of melt temperature setting. According to the DOE analysis, this melt temperature level gives the best mechanical properties of microcellular injection parts [3].

By controlling the cooling rates, the samples with either strong α-form, strong γ-form, or α-γ dual form can be obtained separately, as shown in Figure 8. The XRD results show that the skin regions of both PA-6 microcellular and PA-6 microcellular nanocomposite are all γ-form dominant. The spherulitic structures of the core region of PA-6 microcellular part vary with the molding condition from α–γ dual form to a-form predominant. Compression molded NC2 (5%MMT) specimen with slow cooling can also display the α–γ dual form. But even the core region of injection molded NC2 specimen is still γ-form dominating. However, with the higher nanoclay loading NC3 specimen (7.5%), the crystalline structure of the core region is similar to the case for the BR2 injection molded specimen (Figures 9–11).

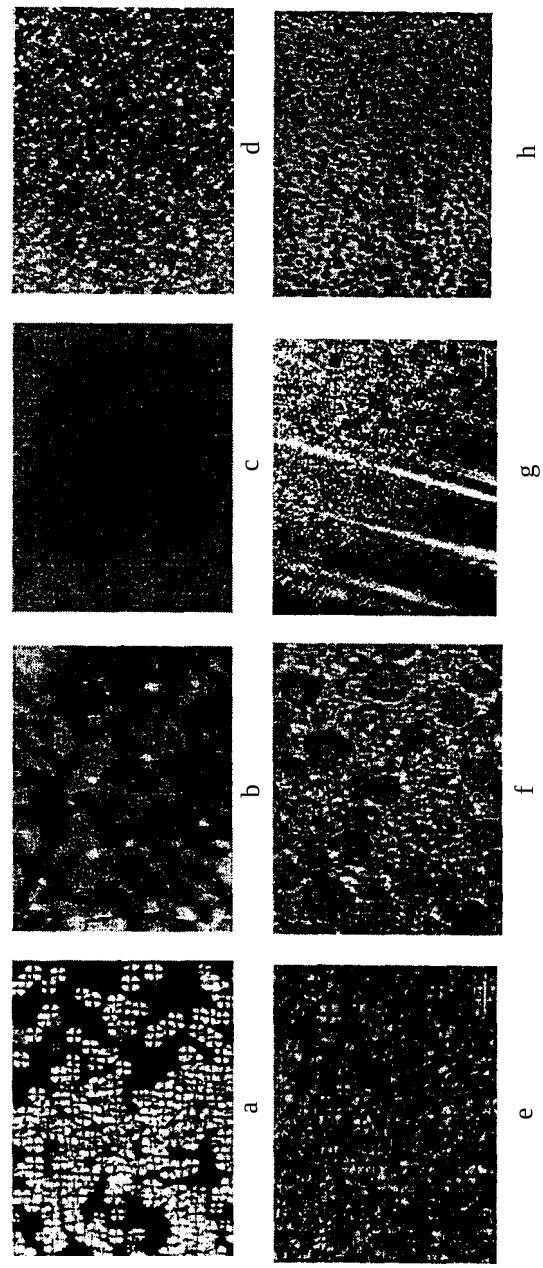

Figure 7. The polarized optical micrographs of hot stage and injection molded specimens: (a) BR2 with fast rate; (b) BR2 with slow rate; (c) NC2 with fast rate; (d) NC2 with slow rate; (e) solid BR2 molded sample; (f) microcellular BR2 molded sample; (g) microcellular BR2 molded sample taken from the corner; and (h) NC2 microcellular molded sample.

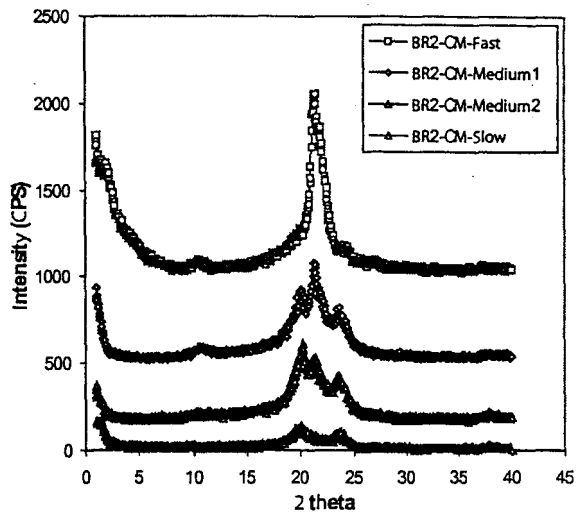

Figure 8. The XRD patterns of BR2 compression molded (CM) samples.

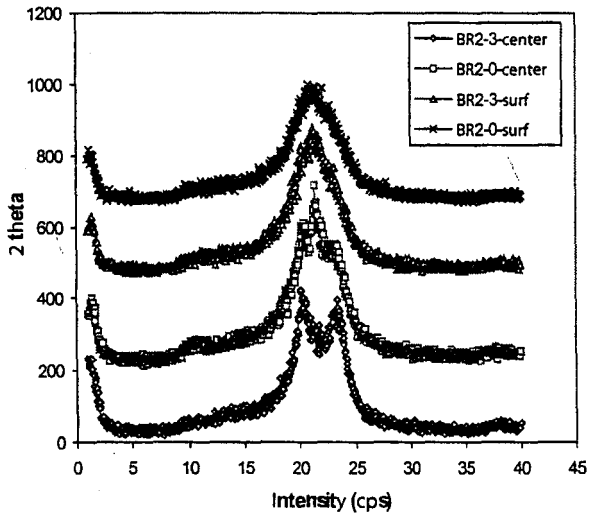

Figure 9. The XRD patterns of BR2 microcellular injection molded samples.

The Avrami equation [4,5] is used to analyze the isothermal crystallization behavior of BR2, NC2, and NC3. It is expressed as

$$X(t) = 1 - \exp[-Kt^n]$$

where K and n are the crystallization constants.

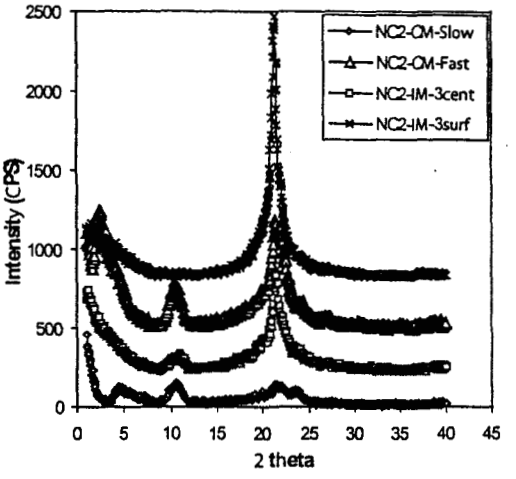

Figure 10. The XRD patterns of NC2 compression molding (CM) microcellular injection molded samples.

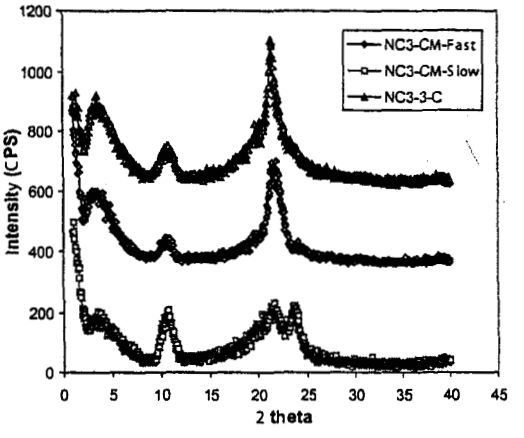

Figure 11. The XRD patterns of NC3 compression molding (CM) and microcellular injection molded samples.

The crystallization rate G is described as the reciprocal of $t_{1/2}$; that is, $G = \tau_{1/2} = t_{1/2}^{-1}$, where the crystallization half-time ($t_{1/2}$), defined as the time at which the extent of crystallization is 50% complete, is determined from the measured parameters.

$$t_{1/2} = \left(\frac{\ln 2}{K}\right)^{1/n}$$

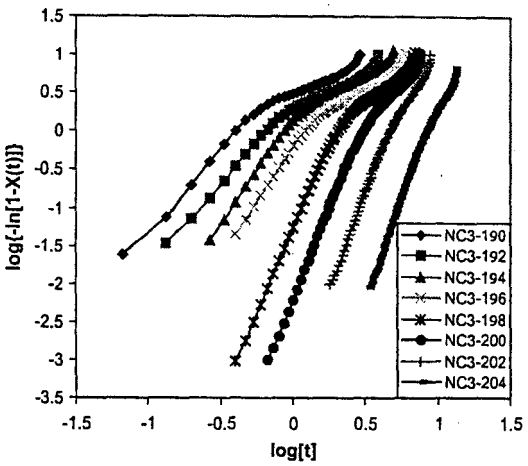

Figure 12. The plots of log{–ln[1–$X(t)$]} vs log[t] for isothermal crystallization of NC3 at different temperatures.

The exemplary result for NC3 is shown in Figure 12. The two-stage crystallization processes can be clearly seen: the primary crystallization stage controlled by nucleation and the secondary crystallization stage governed by crystal growth. Based on the Arrhenius function, the crystallization activation energies for BR2, NC2, and NC3 are determined as 267.62, 362.45, 358.17 kJ/mol. Obviously, NC2 has the highest crystallization activation energy among all the three materials.

The nonisothermal crystallization process is characterized by the following equation [4,5].

$$X(t) = 1 - \exp[-Z_t t^n]$$

where n and Z_t are the rate constants of the nonisothermal crystallization process. They are functions of the cooling rate Φ.

The heat flow curves of BR2, NC2, and NC3 at the cooling rates of 2.5, 5, 10, 20, and 40 K/min are shown in Figure 13. And both the isothermal and nonisothermal results are summarized in Tables 1 and 2, respectively. From Figure 13 and Tables 1 and 2, it can be seen that the nanocomposite NC2 have the highest crystallization rate among all the three materials. The values of n_1 and n_2 indicates that the nucleation mode might contain both homogeneous and heterogeneous mechanisms for NC2 and NC3 at the primary stage. The crystallite impinges and crowds with the neighboring one at the secondary stage. With more addition of nanoclay, the increase of crystallization rate is reduced, as

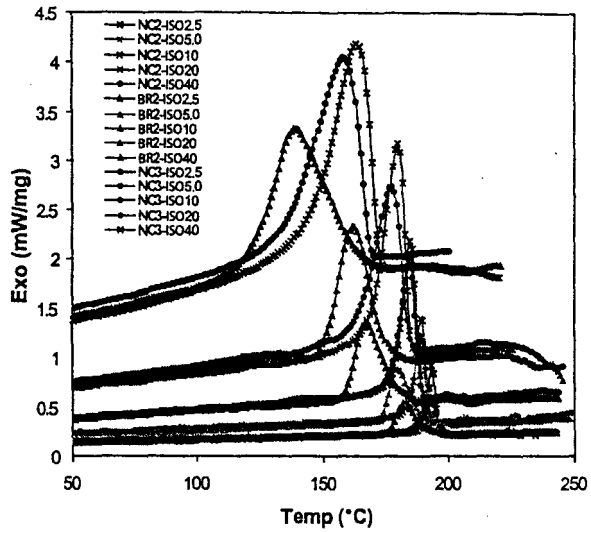

Figure 13. The heat flow vs time during the nonisothermal crystallization processes of BR2, NC2, and NC3 at different cooling rates.

Table 1. Isothermal crystallization constants.

Crystallization temp. (°C)	$\tau_{1/2}$	Crystallization temp. (°C)	$\tau_{1/2}$	Crystallization temp. (°C)	$\tau_{1/2}$
BR2-180	1.81	NC2-190	3.20	NC3-190	2.49
BR2-182	1.39	NC2-192	1.87	NC3-192	1.60
BR2-184	1.06	NC2-194	1.12	NC3-194	1.19
BR2-186	0.757	NC2-196	0.787	NC3-196	0.851
BR2-188	0.581	NC2-198	0.500	NC3-198	0.424
BR2-190	0.368	NC2-200	0.359	NC3-200	0.309
		NC2-202	0.256	NC3-202	0.218
				NC3-204	0.129

Table 2. Nonisothermal crystallization constants.

Cooling rate (K/min)	BR2		NC2		NC3	
	n_1	n_2	n_1	n_2	n_1	n_2
2.5	5.09	2.64	6.69	1.19	4.66	1.62
5	3.96	2.99	6.10	1.62	5.09	1.48
10	4.72	3.17	5.48	1.70	4.63	1.64
20	3.60	3.12	5.28	1.68	4.56	2.39
40	3.79	2.91	4.76	2.17	4.83	2.02

the case for NC3. This agrees well with the XRD, POM, and TEM results mentioned above.

The above results can be explained by the presence of nanoclays in PA-6 matrix, which imposes the space limitation and restriction on the crystalline growth. The huge number of nanoclay platelets dispersed in PA-6 matrix also act as the nucleation agents and promote much more nucleation sites. This leads to smaller and denser crystallite structures.

CONCLUSIONS

With the addition of nanoclays in microcellular injection molded parts, the growth of a-form crystal is suppressed and the formation of γ-form crystals is promoted. Both nanoclay and dissolved gas have a big influence on PA-6 crystalline structures. The existence of nanoclay increases the initial crystallization rate but hampers the crystalline growth at a later stage. But with extra addition of nanoclays in polymer matrix, the increase of crystallization rate is reduced. Nanocomposites with optimal amount of nanoclays possess the maximum crystallization activation energy and produce finer and denser microcell structure which leads to better mechanical properties.

ACKNOWLEDGMENTS

The materials used in the study were generously donated by the RTP Company. Part of this research is supported by the National Science Foundation (DMI-0140396). Experimental assistance from Paul Wilichowski and John Thurlow is acknowledged.

REFERENCES

1. Bureau, M.N., Denuault, J.K., Cole, C. and Enright, G.D. (2002). *Polym. Eng. Sci.*, **42**(9): 1897.
2. Zhang, Z., Nawaby, Z.V. and Day, M.J. (2003). *Polym. Sci., Part B, Polym. Phys.*, **41**: 1518.
3. Yuan, M., et al. (2004). *Polym. Eng. Sci.*, **44**(4): 673.
4. Jeziorny, A. (1978). *Polymer*, **19**: 1142.
5. Zhang, Q., Zhang, Z., Zhang, H. and Mo, Z. (2002). *J. Polym. Sci.*, **40**: 1784.